https://doi.org/10.20965/ijat.2019.p0432

Paper:

Feasibility Study of a Hybrid Spindle System with Ball and Active Magnetic Bearings for Quadrant Glitch Compensation During End Milling

Mitsunari Oda*,†, Takashi Torihara, Eiji Kondo**, and Noriyoshi Kumazawa****

*Makino Milling Machine Co., Ltd.
4023 Nakatsu, Aikawa-Machi, Aiko-Gun, Kanagawa 243-0303, Japan
†Corresponding author, E-mail: odam@makino.co.jp
**Kagoshima University, Kagoshima, Japan

[Received June 23, 2018; accepted March 25, 2019]

Quadrant glitches are caused by friction and motion loss on the feed axis of machine tools. A previously developed method of compensating for quadrant glitches using the feed axis in which the friction model and time series data are not consistent with the actual friction behavior has some problems, making it difficult to construct a feedback system with a high response problems such as a feed axis with a large lost motion. The ultimate goal of this study is to develop an innovative method of compensating for the quadrant glitches caused by the motion of the feed axis of the machine tool using a newly proposed hybrid spindle system with an active magnetic bearing at the end near the end mill and a ball bearing at the other end in combination with a proportional-integral-derivative controller. This study aims to verify the effectiveness of the proposed quadrant glitch compensation method through experiments on the motion of the end mill using a model experimental device for the hybrid spindle system. Through experiments, a quadrant glitch with a peak of 7 μm without compensation is decreased to 1 μm by applying the proposed method using the hybrid spindle system. The undercut error is also decreased by applying the proposed method.

Keywords: end milling, quadrant glitch compensation, hybrid spindle system, active magnetic bearing, ball bearing

1. Introduction

Machine tools used at production sites must have high accuracy and productivity. However, the machining error, called quadrant glitch, reduces the accuracy of product machining. Quadrant glitches are caused by friction and motion loss on the feed axis. Numerous studies have been conducted regarding compensating for quadrant glitches and patents for compensation methods [1–9]. A rigorous model of the friction [2–4] and stored time series friction data obtained by repeat control [5] could compensate for quadrant glitches; however, these methods are not effective when the friction model or time series data are not consistent with the actual friction. A high-sensitivity feedback system could lower the friction to reduce the occurrence of quadrant glitches, but the capability of such a compensation is not sufficient in cases where constructing a feedback system with a high response (e.g., for a feed axis with a large lost motion) is difficult [6, 7]. Machined parts are fabricated by the relative motion between a workpiece and a tool during machining. Consequently, in principle, quadrant glitches could be compensated for by the motion of an end mill instead of a table. However, using the motion of an end mill to compensate for the quadrant glitches has not been tried in previous studies.

As an alternative, rolling bearings, particularly ball bearings, have been widely adopted as machine tool spindles because of their performance and high reliability [10, 11]. Active magnetic bearing spindles, which are supported by active magnetic bearings, are superior to other types of bearing spindle systems in terms of functionality. They can control the offset of the rotary axis and the stiffness and damping of the spindle system [12–19]. However, active magnetic bearing spindle systems have some disadvantages, including a load capacity smaller than that of the rolling bearings, limited capacity for performance improvement by control systems, and high price [20]. Consequently, the active magnetic bearing spindle system is not suitable for the compensation of quadrant glitches, although it could compensate for a quadrant glitch. A spindle system with a simpler and inexpensive control system, that can compensate for quadrant glitches, is expected to be functional for a larger cutting force.

The ultimate goal of this study is to develop an innovative method of compensating for quadrant glitches that is effective, regardless of the modeling accuracy and the lost motion of the feed axis. In the proposed method, a hybrid spindle system with an active magnetic bearing at the end near the end mill and a ball bearing at the other end is newly proposed to compensate for the quadrant glitches caused by the motion of the feed axis of the machine tool

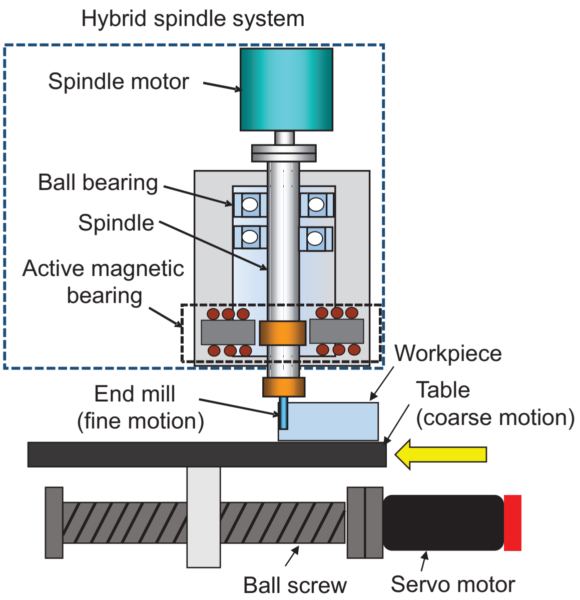

Fig. 1. Conceptual diagram of the proposed quadrant glitch compensation method.

table [21]. The end mill could be driven by the electromagnetic force of the active magnetic bearing. This machining system consists of the hybrid spindle system as a fine motion device and the machine tool table as a coarse motion device. The hybrid spindle system can compensate for the quadrant glitches caused by the motion error of the machine tool table. This study aims to verify the effectiveness of the proposed quadrant glitch compensation method through experiments on the motion of the end mill using a model experimental device for the hybrid spindle system.

2. Quadrant Glitch Compensation Method Using the Proposed System

Figure 1 shows a conceptual diagram of the proposed compensation method of the quadrant glitch using the proposed hybrid spindle system with an active magnetic bearing near the end mill and a ball bearing at the other end. The proposed hybrid spindle system enables fine motion control, as shown in **Fig. 1**. The hybrid spindle system consisting of a spindle, an active magnetic bearing, and a rolling bearing can compensate for the quadrant glitches caused by the friction and lost motion on the feed axis of the table, which is a coarse motion device.

3. Model Experimental Device for the Hybrid Spindle System

Figure 2 shows the model experimental device for the proposed hybrid spindle system used herein. The model device consisted of a spindle head as the rolling bearing, a tool holder as the spindle, an active magnetic bearing,

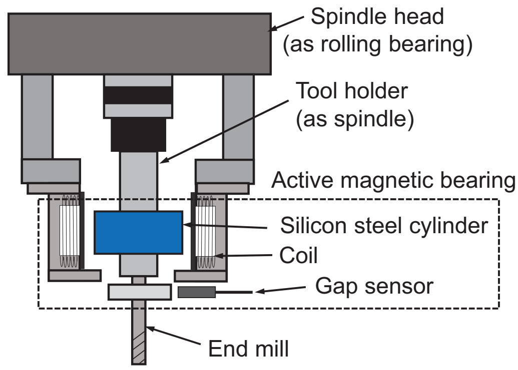

Fig. 2. Model experimental device for the hybrid spindle system.

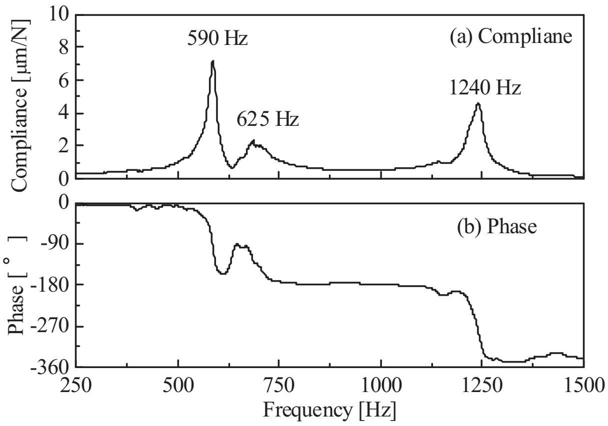

Fig. 3. Frequency response function of the silicon steel cylinder.

and an end mill. The active magnetic bearing consisted of a silicon steel cylinder subjected to an electromagnetic force, an aluminum ring, and electromagnetic coils. The electromagnetic coils were fixed with a jig to the spindle head to maintain a constant clearance between the electromagnetic coils and the silicon steel cylinder.

First, the free vibration parameters of a dummy spindle were measured through impact tests, in which the silicon steel cylinder was impacted by an impulse hummer. The frequency response function was calculated from the measured impact force and acceleration signals of the silicon steel cylinder using the fast Fourier transform (FFT). **Fig. 3** shows the frequency response function of the cylinder. The compliance and the phase are plotted against the frequency in the upper and lower parts of **Fig. 3**, respectively. Three peaks were found in the compliance at frequencies of 590, 625, and 1240 Hz. Consequently, the silicon steel cylinder vibrated in the same phase with the end mill at the first-order natural frequency of 590 Hz. Moreover, the end mill vibrated in the reverse phase with the silicon steel cylinder at the second-order natural frequency of 625 Hz.

Figure 4 shows the relationship between the load and the deflection of the spindle at the silicon steel cylinder shown in **Fig. 2** when the deflection was gradually increased and then decreased. Note that **Fig. 4** only

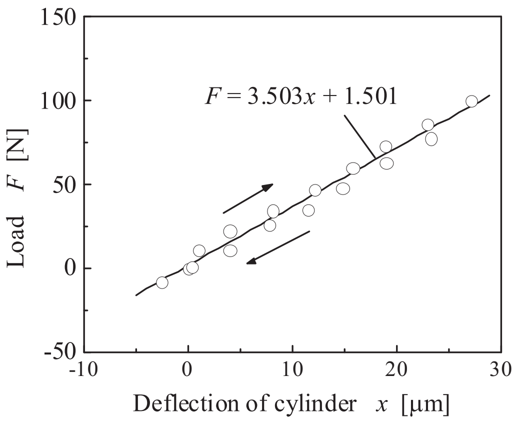

Fig. 4. Stiffness of the spindle at the silicon steel cylinder.

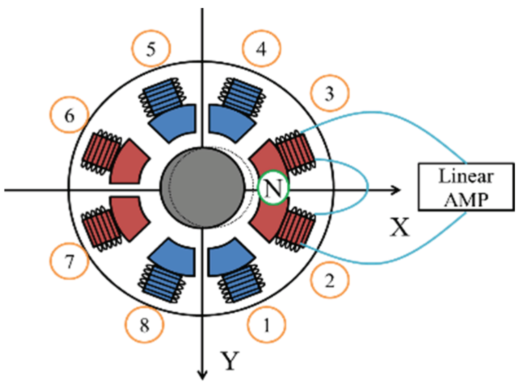

Fig. 5. Arrangement of the electromagnetic coils.

shows the relationship of the X-axis' direction because the Y-axis' direction features the same relationship. The load was measured using a dynamometer with a jig. The deflection was measured using a laser displacement sensor. The load measured for the increasing deflection was somewhat larger than that measured for the decreasing deflection at all deflection values. The slope of the linear load-deflection relationship obtained using the method of least squares, which was also plotted in **Fig. 4**, was the spring constant of the spindle at the silicon steel cylinder that was 3.503 N/μm.

Figure 5 shows the circular arrangement of the eight poles of the electromagnetic coils in the active magnetic bearing. Each coil was numbered from ① to ⑧. Each pair of coils (e.g., ② and ③) was connected as one set in a series, such that the position of coils ② and ③ coincided with the positive X-direction of the machine tool table and that of coils ⑥ and ⑦ coincided with the negative X-direction.

Figure 6 illustrates a conceptual diagram of the electromagnetic device in the case where the electromagnet magnetized by the electromagnetic coils carrying an electric current to the north pole moves the silicon steel cylinder to the right-hand side. In **Fig. 6**, i denotes the current along the right-hand electromagnetic coil, while e stands for the input voltage of the switching circuit. If the elec-

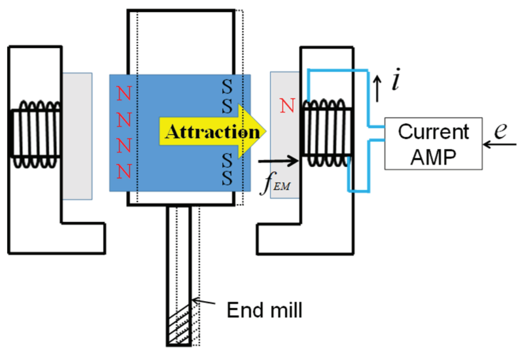

Fig. 6. Conceptual diagram of the electromagnetic.

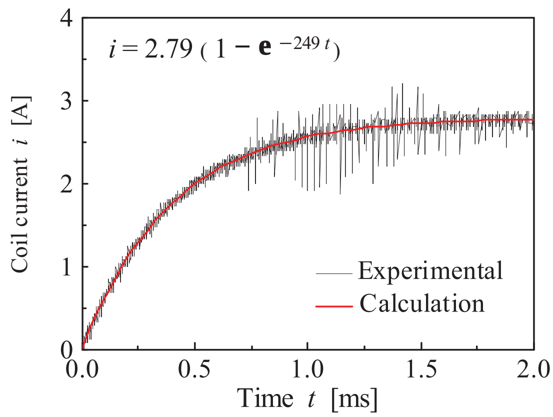

Fig. 7. Step response current of the magnetic coil.

tromagnet is magnetized such that the north pole is on its right, the silicon steel cylinder is magnetized with the south pole on its right, generating an attractive electromagnetic force that displaces the end mill to the right.

The voltage e applied to the electromagnetic coil by the linear amplifier is expressed as

$$e = L_c \frac{\mathrm{d}i}{\mathrm{d}t} + R_c i, \quad . \quad . \quad . \quad . \quad . \quad . \quad . \quad . \quad . \quad . \quad . \quad . \quad (1)$$

where L_c and R_c are the inductance measured at the installation location and the resistance of the electromagnetic coil, respectively. The following equation can be derived by solving Eq. (1) under the assumption that the voltage e is a step function of magnitude E_1:

$$i = \frac{E_1}{R_c}\left(1 - \mathrm{e}^{\frac{t}{T}}\right), \quad . \quad . \quad . \quad . \quad . \quad . \quad . \quad . \quad . \quad . \quad . \quad (2)$$

where T is defined as L_c/R_c. This model has a first-order lag. The R_c and T values can be determined by measuring the step response of the current.

Figure 7 shows the experimental results for the step response of the current passing through the magnetic coil with an input voltage E_1 of 2.4 V. The equation shown in **Fig. 7** was derived from the measured response using the nonlinear least squares method and is given as:

$$i = 2.79\left(1 - \mathrm{e}^{-249t}\right). \quad . \quad . \quad . \quad . \quad . \quad . \quad . \quad . \quad . \quad . \quad . \quad (3)$$

A comparison of Eqs. (2) and (3) revealed that the R_c,

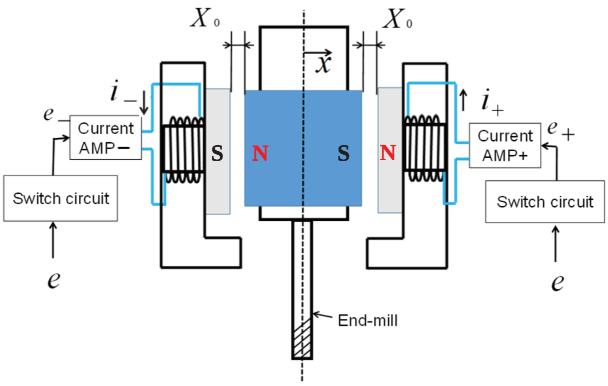

Fig. 8. Conceptual figure of the active magnetic bearing.

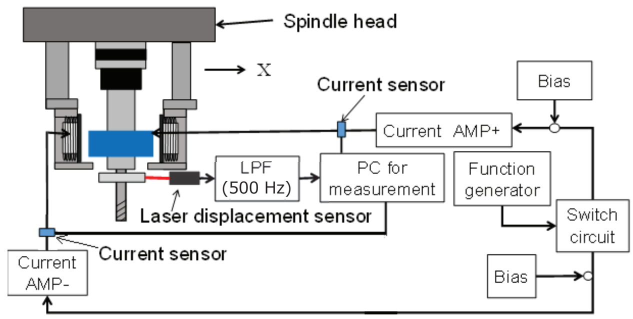

Fig. 9. Experimental apparatus for the measurement of the relationship between the electromagnetic force and the current.

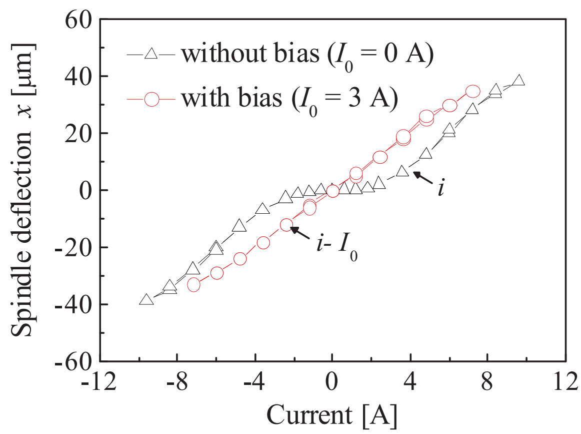

Fig. 10. Relationship between the tool displacement and the pulsed input current amplitude.

T, and L values were 0.86 Ω, 0.4 ms, and 0.34 mH, respectively.

Figure 8 shows a conceptual diagram of the active magnetic device with bias currents. In **Fig. 8**, i_+ and i_- are the currents passing through the electromagnetic coils on the right and left sides of the cylinder, respectively; X_0 is the clearance between the electromagnetic coils and the outer surface of the silicon steel cylinder; e is the input voltage of the switch circuit; e_+ and e_- are the output voltages from the right and left switch circuits, respectively; and x is the end mill displacement. If an electromagnet to the right of the silicon steel cylinder is magnetized such that the north pole is facing the cylinder, the cylinder is magnetized such that the south pole is facing the electromagnet, and the resulting attractive electromagnetic force causes the end mill to move to the right. This active magnetic bearing has a switch circuit to switch the attractive force producing this motion from side to side.

The electromagnetic force f_{EM} is expressed as:

$$f_{EM} = K_{EM}\left\{\frac{i_+^2}{(X_0-x)^2} - \frac{i_-^2}{(X_0+x)^2}\right\}, \quad . \quad . \quad . \quad (4)$$

where K_{EM} is the electromagnetic force coefficient. The sensitivity of the electromagnetic force was low when the input voltages e_+ and e_- of the current amplifiers, which were proportional to the input currents i_+ and i_- of the coils, were near zero because the electromagnetic force increased with the square of the currents, as shown in Eq. (4). The relationship between the electromagnetic force f_{EM} and the input current was linearized by adding a bias current such that the sensitivity of the electromagnetic force to the changes in the current was higher for the input currents near zero. The linearized electromagnetic force is given by:

$$f_{EN} = K_{EM}\left\{\frac{(I_0+i_+)^2}{(X_0-x)^2} - \frac{(I_0-i_-)^2}{(X_0+x)^2}\right\}, \quad . \quad . \quad . \quad (5)$$

where I_0 is the bias current.

Figure 9 shows the experimental apparatus for the measurement of the relationship between the electromagnetic force and the current of the active magnetic bearing. The spindle displacement was measured using a laser displacement sensor. The coil current was measured using a current sensor. In this experiment, the pulsed input voltage e from the function generator was applied to the switch circuit. **Fig. 10** depicts the experimental results of the relationship between the spindle deflection and the amplitude of the pulsed current without the bias current I_0. As shown in **Fig. 10**, the obtained relationship between the spindle deflection and the coil current was linearized around the origin with the addition of the bias current I_0. The spindle deflection between −22 and 22 µm was proportional to the current between −4.8 and 4.8 A.

4. Design and Evaluation of the Control System for the Active Magnetic Bearing

4.1. Control System Requirements

The X-Y table was moved along a circular path 20 mm in diameter with a high acceleration (1.78 m/s^2) at a speed of 8000 mm/min to generate a quadrant glitch along the X-axis (**Fig. 1**). **Fig. 11** shows the shape of the resulting quadrant glitch. The shape of the quadrant glitch was obtained as the difference between the measured position of the table in the X-direction by the grid encoder equipment and the target position at the moment when the X-axis

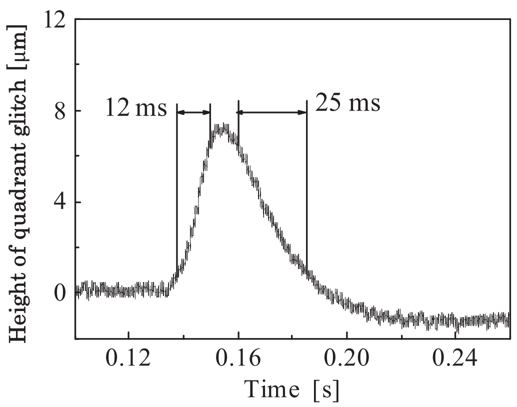

Fig. 11. Quadrant glitch occurring on the X-axis with the X-Y table moving in a circular motion.

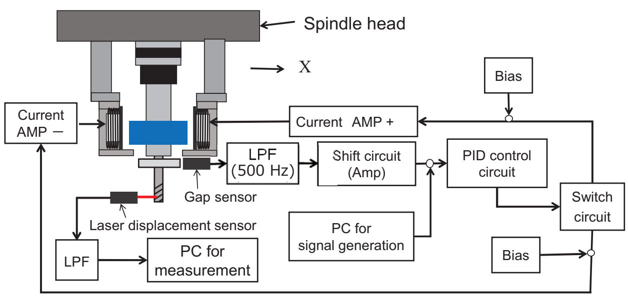

Fig. 12. Experimental control system of the active magnetic bearing with PID control.

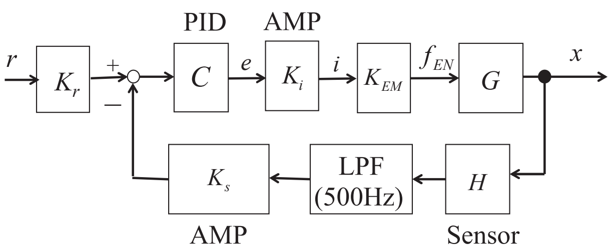

Fig. 13. Block diagram of the controller of the active magnetic bearing with PID control.

rotation reversed. As shown in **Fig. 11**, the rise time of the quadrant glitch from 10% to 90% of the local maximum value was approximately 12 ms, while the fall time of the quadrant glitch from 90% to 10% was approximately 25 ms.

4.2. Control System with PID Control

Figure 12 shows the control system for the active magnetic bearing with an analog proportional-integral-derivative (PID) control circuit composed of operational amplifiers. A low-pass filter of 500 Hz was inserted in the feedback loop of the displacement sensor for the silicon steel cylinder shown in **Figs. 12** and **13** to make tuning the PID control system easier. An input signal was generated by a personal computer (PC). The displacement of the lower end of the end mill was measured using a laser

Table 1. Gains of the PID controller.

Type of controller	K_P [V/m]	K_I [V/(m·s)]	K_D [V·s/m]
PID	2.79	190	0.0013

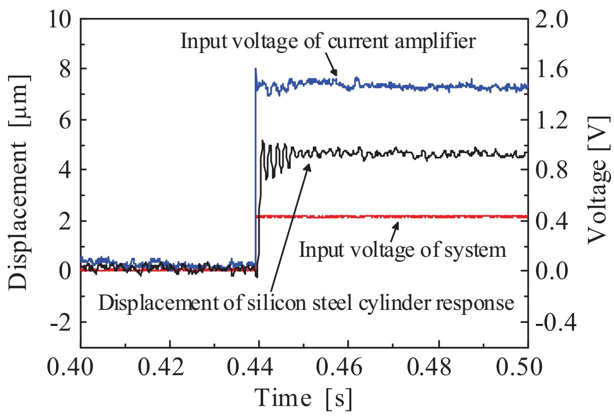

Fig. 14. Rising step response of the silicon steel cylinder.

displacement sensor. **Fig. 13** shows a block diagram of the control system in **Fig. 12.** In **Fig. 13**, r is the displacement input into the control system; e is the voltage input into the current amplifier; and x is the aluminum ring displacement proportional to that of the silicon steel cylinder. The block labeled C shows the PID circuit described as:

$$C = K_P + \frac{K_I}{s} + K_D s, \quad \ldots \ldots \ldots \ldots \quad (6)$$

where K_P, K_I, and K_D are the proportional, integral, and differential gains, respectively. The values of the K_P, K_I, and K_D coefficients in the PID controller were determined by trial and error while referring to the limit sensitivity method (**Table 1**). In **Fig. 13**, G is the frequency response function of the spindle at the silicon steel cylinder, while K_i, K_{EM}, K_s, and H are the gains. K_r is a coefficient used to convert displacement to voltage. An LPF of 500 Hz was inserted into the feedback loop to avoid the spillover at the natural frequencies discussed earlier and given in **Fig. 3**.

Figure 14 shows the experimental rising step response of the silicon steel cylinder to the step input voltage plotted as a red line in the figure. The experiments were performed without spindle rotation to measure the end mill displacement at the lower end with high precision. The step response to the input of the control circuit was generated by the PC used for signal generation in **Fig. 12**. The obtained input voltage of the current amplifier plotted as a blue line in **Fig. 14** rapidly reached the target value of the rising step, although the response showed a few oscillations at the beginning. The obtained silicon steel cylinder response exhibited oscillations at the moment the input increased. The frequency of the vibration coincided approximately with the first-order natural frequency given in **Fig. 3** because the vibrations at the second-order natural frequency were suppressed by the magnetic force of the active magnetic bearing. The rise time of the obtained

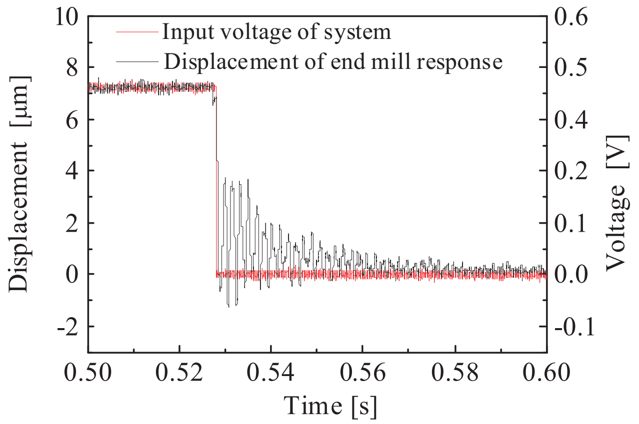

Fig. 15. Rising step response of the lower end of the end mill.

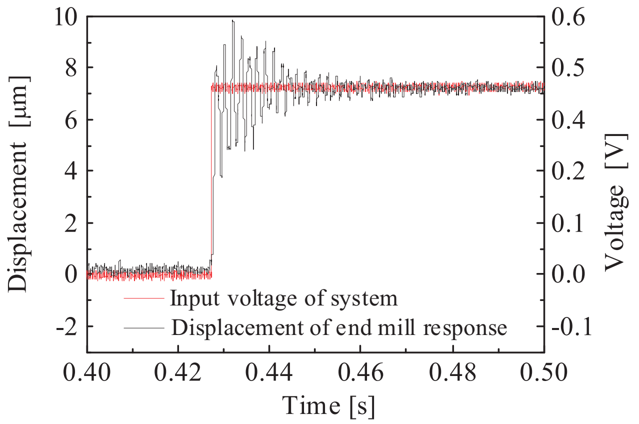

Fig. 16. Falling step response of the lower end of the end mill.

step response shown in **Fig. 14** was approximately 1 ms, although the response showed oscillations.

Figure 15 shows the experimental rising step response of the lower end of the end mill to the step input voltage plotted as a red line in **Fig. 15**. The obtained response showed severe oscillations at the moment when the input increased. The frequency of the vibration approximately coincided with the first-order natural frequency given in **Fig. 3**. Consequently, the free vibrations at the first-order natural frequency could have been induced by the step motion of the silicon steel cylinder driven by the step input because the end of the end mill was not restrained. The rise time of the obtained step response shown in **Fig. 15** was approximately 2 ms; thus, although the response showed a severe oscillation, it was less than half of the rise time (12 ms) of the quadrant glitch shown in **Fig. 11**. This result demonstrated that the proposed hybrid spindle system with PID control is capable of achieving a sufficiently rapid response to compensate for the machining error caused by the quadrant glitches like that shown in **Fig. 11**.

Figure 16 shows the falling experimental step response of the lower end of the end mill to the step input voltage plotted as a red line in the figure. The obtained response showed severe oscillations at the moment when the input

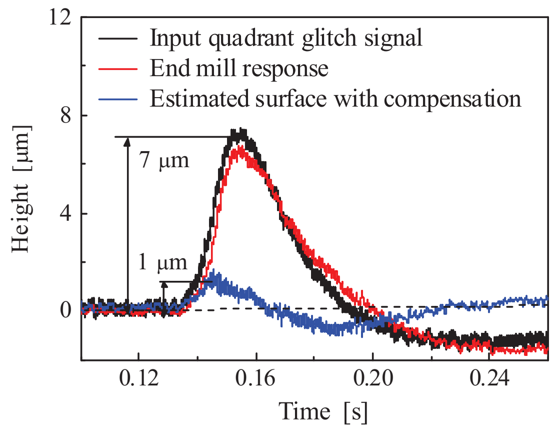

Fig. 17. Response of the hybrid spindle system with PID control to an input signal of a quadrant glitch.

decreased. The fall time of the obtained step response shown in **Fig. 16** was approximately 3 ms; thus, although the response showed severe oscillations, the response time was sufficiently less than the fall time (25 ms) of the quadrant glitch shown in **Fig. 11**. However, it was longer than the rise time of the step response to the rising input voltage shown in **Fig. 15**. The response of the system at an input voltage near 0 V may be considered to contain a nonlinearity caused by the switch circuits.

Figure 17 shows the experimental response of the lower end of the end mill shown in **Fig. 12** to the input quadrant glitch signal plotted as a black line in the case where the hybrid spindle system with the PID controller was implemented. The input quadrant glitch signal was also generated from the PC for signal generation, where the height of the quadrant glitch in **Fig. 11** was converted to the voltage through the use of K_r identified by the relationship between the input voltage of the step and the displacement shown in **Figs. 14** and **15**. The obtained response at the lower end of the end mill, which was plotted as a red line, approximately traced the shape of the input quadrant glitch signal, but with a lag of approximately 2 ms. The final machined surface with compensation by the proposed system, which is represented by the blue line, was estimated as the difference between the input quadrant glitch signal and the response in **Fig. 17**. The maximum machining error with compensation by the hybrid spindle system with the PID controller was 1 μm, which was substantially smaller than the maximum quadrant glitch of 7 μm. The maximum undercut error with the compensation, which occurred at approximately 0.19 s, was also smaller than the maximum undercut caused by the quadrant glitch, which occurred at approximately 0.24 s.

5. Conclusion

This study proposed the concept of an innovative method of compensating for the quadrant glitches caused by the motion of the feed axis of a machine tool. A hybrid spindle system with an active magnetic bearing at the end near the end mill and a ball bearing at the other end, including a PID controller, was newly proposed to compensate for the quadrant glitches. The experiments conducted to demonstrate the compensation performance of the proposed hybrid spindle system showed that the maximum machining error from a quadrant glitch of 7 μm was decreased to 1 μm when the hybrid spindle system was applied. The undercut error was also decreased by applying the proposed hybrid spindle system.

References:

[1] R. Sato, "Compensation Techniques for Quadrant Glitches on Circular Trajectories," Proc. of 2007 JSPE Autumn Meeting, pp. 691-692, 2007 (in Japanese).

[2] R. Sato, Y. Terashima, and M. Tsutsumi, "Quadrant Glitch Compensator Based on Friction Characteristics in Microscopic Region," J. of JSPE, Vol.74, No.6, pp. 622-626, 2008 (in Japanese).

[3] Z. Jamaludin, H. van Brussel, G. Pipeleers, and J. Swevers, "Accurate Motion Control of XY High-Speed Linear Drives using Friction Model Feedforward and Cutting Forces Estimation," CIRP Annals. Manufacturing Technology, Vol.57, No.1, pp. 403-406, 2008.

[4] N. A. Rafan, Z. Jamaludin, T. H. Chiew, L. Abdullah, and M. N. Maslan, "Contour Error Analysis of Precise Positioning for Ball Screw Driven Stage Using Friction Model Feedforward," Procedia CIRP, Vol.26, pp. 712-717, 2015.

[5] H. Iwashita, H. Kawamura, and Z. Tang, "Control device to be driven by servo motor," J. P. Patent 3805309, 2004.

[6] H. Itagaki, M. Tsutsumi, and H. Iwanaka, "Improvement of Response Characteristics of Linear Motor Servo Systems Using Virtual Friction," Proc. of Int. Conf. on Leading Edge Manufacturing in 21st century, 3344, 2011.

[7] Z. Jamaludin, H. van Brussel, and J. Swevers, "Tracking performances of cascade and sliding mode controllers with application to a XY milling table," Proc. of ISMA2006, pp. 81-92, 2006.

[8] T. Higuchi, Y. Manabe, R. Sato, and M. Tsutsumi, "Study on Motion Accuracy Enhancement in NC Machine Tools: Development of Autonomous Quadrant Glitch Compensator Corresponding to Torque Change," J. of JSPE, Vol.76, No.5, pp. 535-540, 2010 (in Japanese).

[9] R. Sato, "Generation Mechanism of Quadrant Glitches and Compensation for it in Feed Drive System of NC Machine Tools," Int. J. Automation Technol., Vol.6, No.2, pp. 154-162, 2012.

[10] E. Abel, Y. Altintas, and C. Brecher, "Machine Tool Spindle Units," CIRP Annals – Manufacturing Technology, Vol.59, No.2, pp. 781-802, 2010.

[11] K. Kakuta, "Ultra-high speed rolling bearings," J. of JSPE, Vol.53, No.7, pp. 1005-1008, 1987 (in Japanese).

[12] S. Goto, A. Matsubara, I. Yamaji, and S. Ishii, "Development of a contactless biaxial magnetic loader for evaluation of spindle dynamics," Proc. the 9th Int. Conf. on Leading Edge Manufacturing in 21st Century, C90, 2017.

[13] T. Huang, Z. Chen, H.-T. Zhang, and H. Ding, "Active Control of an Active Magnetic Bearings Supported Spindle for Chatter Suppression in Milling Process," J. of Dynamic Systems, Measurement, and Control, Vol.137, No.11, 111003, 2015.

[14] H. Cao, X. Zhang, and X. Chen, "The concept and progress of intelligent spindles: A review," Int. J. of Machine Tools and Manufacture, Vol.112, pp. 21-52, 2017.

[15] F. Chen and G. Liu, "Active damping of machine tool vibrations and cutting force measurement with a magnetic actuator," The Int. J. of Advanced Manufacturing Technology, Vol.89, pp. 691-700, 2017.

[16] H.-J. Ahn, S. Jeon, and D.-C. Han, "Error analysis of the cylindrical capacitive sensor for active magnetic bearing spindles," J. of Dynamic Systems, Vol.122, pp. 102-107, 2000.

[17] A. C. Wroblewski, J. T. Sawicki, and A. H. Pesch, "Rotor Model Updating and Validation for an Active Magnetic Bearing Based High-Speed Machining Spindle," J. of Engineering for Gas Turbines and Power, Vol.134, 2012.

[18] M. H. Kimman, H. H. Langen, and R. H. Munnig Schmidt, "A miniature milling spindle with Active Magnetic Bearings," Mechatronics, Vol.20, pp. 224-235, 2010.

[19] J. T. Sawicki, E. H. Maslen, and K. R. Bischof, "Modeling and Performance Evaluation of Machining Spindle with Active Magnetic Bearings," J. of Mechanical Science and Technology, Vol.21, pp. 847-850, 2007.

[20] G. Schweitzer, "Active magnetic bearings – chances and limitations," IFToMM 6th Int. Conf. on Rotorx, 2002.

[21] M. Oda, T. Torihara, and E. Kondo, "Development of Small Displacement Device of End-mill at Cutting Point using Electro-magnetic Force," Proc. the 9th Int. Conf. on Leading Edge Manufacturing in 21st Century, C27, 2017.

Name:
Mitsunari Oda

Affiliation:
Senior Specialist, Research & Development, Makino Milling Machine Co., Ltd.

Address:
4023 Nakatsu, Aikawa-Machi, Aiko-Gun, Kanagawa 243-0303, Japan

Brief Biographical History:

1994- Makino Milling Machine Co., Ltd.

Main Works:

- "Development of Small Displacement Device of End-mill at Cutting Point using Electro-magnetic Force," Proc. the 9th Int. Conf. on Leading Edge Manufacturing in 21st Century, C27, 2017.
- "Feasibility study of hybrid spindle system with ball and electromagnetic bearings for suppression of chatter vibrations during milling with a small end mill," Proc. the 18th Int. Conf. of European Society for Precision Engineering and Nanotechnology, pp. 219-220, 2018.

Membership in Academic Societies:

- International Academy for Production Engineering (CIRP)
- Japan Society for Precision Engineering (JSPE)
- Japan Society of Mechanical Engineers (JSME)

Name:
Takashi Torihara

Affiliation:
Toyota Motor Kyushu, Inc.

Address:
1 Kamiaruki, Miyawaka city, Fukuoka 823-0015, Japan

Brief Biographical History:

2017- Toyota Motor Kyushu, Inc.

Name:
Eiji Kondo

Affiliation:
Professor, Graduate School of Science and Engineering, Kagoshima University

Address:
1-21-40 Korimoto, Kagoshima, Kagoshima 890-0065, Japan

Brief Biographical History:
1980- Nippondenso Co., Ltd.
1982- Komatsu Ltd.
1985- National Institute of Technology, Toyota College
1996- Kagoshima University

Main Works:
- "A New Method to Detect Regenerative Chatter Using Spectral Analysis, Part 1: Basic Study on Criterion for Detection of Chatter," ASME J. Manufacturing Science and Engineering, Vol.119, pp. 461-466, 1997.
- "Monitoring of Tool Wear of Single Crystal Diamond Tool in Ultra-Precision Cutting of Aluminum Alloy (1st Report) – Consideration of Effective Parameters in Indirect Method for Monitoring of Tool Wear," J. of Japan Society for Precision Engineering, Vol.75, No.6, pp. 757-761, 2009.
- "Cutting performance of two-layered cutting tool tips with thin M20 and K10 sintered carbide plates compared to homogeneous tips," Int. J. of Machine Tools & Manufacture, Vol.49, pp. 1048-1052, 2009.

Membership in Academic Societies:
- Japan Society of Mechanical Engineers (JSME)
- Japan Society for Precision Engineering (JSPE)
- Society of Instrument and Control Engineers (SICE)

Name:
Noriyoshi Kumazawa

Affiliation:
Associate Professor, Department of Mechanical Engineering, Kagoshima University

Address:
1-21-40 Korimoto, Kagoshima, Kagoshima 890-0065, Japan

Brief Biographical History:
1996- Kagoshima University
2012-2013 Visiting Scholar, University of California, Berkeley

Main Works:
- "Novel Concept to Detect an Optimum Thixoforming Condition of Al-Al3Ni Functionally Graded Material by Wavelet Analysis for Online Operation," Materials, Vol.4, No.12, pp. 2183-2196, 2011.

Membership in Academic Societies:
- Japan Society of Mechanical Engineers (JSME)
- Society of Instrument and Control Engineers (SICE)
- Institute of Systems, Control and Information Engineers (ISCIE)